THE ASTROPHYSICAL JOURNAL, 402:537–545, 1993 January 10

FIRST MEASUREMENTS OF EXTRAGALACTIC CO(4–3)

R. GÜSTEN,[1,2] E. SERABYN,[2] C. KASEMANN,[1] A. SCHINCKEL,[3]
G. SCHNEIDER,[1] A. SCHULZ,[4] AND K. YOUNG[2]

Received 1992 April 20; accepted 1992 July 14

ABSTRACT

We report the first measurements of extragalactic CO(4–3) toward a sample of prominent nearby galactic nuclei (NGC 253, IC 342, M82, and NGC 6946). With the $J = 4$ level 55 K above ground, and critical densities for excitation of order $\sim 10^4$–10^5 cm^{-3}, detection of the CO(4–3) line provides direct evidence for large amounts of warm, dense molecular gas. A multitransition CO excitation analysis, based on all presently observed ^{12}CO and ^{13}CO transitions up to $J = 6-5$, has been performed to confine the physical state of the gas. Single-component homogeneous models fail to fit the observations. As a next approximation, simple two-component models provide good matches to the observations, with a warm, dense, compact phase superposed on extended, less excited gas. The decomposition suggests that M82 (and likely NGC 253) harbors comparable masses of the warm and dense ($\sim$50–70 K, $\sim 10^{4-5}$ cm^{-3}), and low-excitation ($T \cdot n^{1/2} \sim 8 \times 10^2$) phases, $\sim 10^8$ $M_\odot$ each. Toward IC 342, our excitation study determines the average properties of the massive molecular clouds and the more extensive "intercloud" medium seen in recent interferometric maps. The massive clouds ($\sim 10^6$ $M_\odot$ each) are dense ($\sim 2 \times 10^4$ cm^{-3}) and warm (50–70 K), resembling those in the center of our Galaxy. While the highly excited gas phase in M82 (and NGC 253) is likely related to nuclear star formation activity and concomitant high UV flux, for the more moderate excitation conditions in IC 342 (and NGC 6946), large-scale heating processes, such as the dissipation of turbulence, may be viable.

Subject headings: galaxies: ISM — galaxies: nuclei — ISM: molecules

1. INTRODUCTION

The molecular gas in galactic nuclei is generally warmer and denser than in more quiescient galactic disk clouds (e.g., Henkel, Baan, & Mauersberger 1991). However, most of the evidence for this more excited gas phase comes from low-excitation transitions of CO, as well as only a few other species, e.g., NH_3 (Ho et al. 1990), CS (Mauersberger, Henkel, & Sage 1990), and HCN (Downes et al. 1992). With generally only single, or few, transitions observed per molecule, it is necessary to ask how representative of the bulk gas properties the physical parameters (density, temperature) deduced from these observations are.

The full range of densities and temperatures present in molecular gas is best explored via a multitransition excitation analysis, using preferably an ubiquitous molecule such as CO, which provides many potentially observable transitions probing a wide range of excitation conditions. Extragalactic excitation studies have thus far concentrated mainly on the first few CO rotational transitions, but recent progress in submillimeter telescope and receiver technology has enabled the study of a number of higher rotational CO transitions. Here we report the first measurements of extragalactic CO(4–3) emission from four nearby galactic nuclei, which complement the CO(6–5) study by Harris et al. (1991) of the same objects. With a temperature above ground of 55 K for the $J = 4$ level and a critical density for excitation of $\sim 10^4$–10^5 cm^{-3}, the CO(4–3) line intensity provides important constraints on both the warm, dense circumnuclear molecular gas, and the lower excitation "intercloud" phase.

[1] Max-Planck-Institut für Radioastronomie, Auf dem Hügel 69, 5300 Bonn, Germany.
[2] California Insititute of Technology, 320-47, Pasadena, CA 91125.
[3] Caltech Submillimeter Observatory, 1059 Kilauea Avenue, Hilo, HI 96720
[4] I. Physik. Institut der Universität zu Köln, Zülpicherstr 77, 5000 Köln 1, Germany

2. OBSERVATIONS AND RESULTS

The observations were made during 1990 October 24–31 with the MPIfR 460 GHz Schottky receiver (Keen et al. 1986) installed at the Cassegrain focus of the CSO 10.4 m telescope. T_{RX} was $\sim$1150 K DSB, and excellent atmospheric conditions (zenith opacities as low as $\tau_{460} \sim 0.6$) provided total system temperatures, including atmospheric losses, of $T_{sys} \sim 7000$ K. Simultaneous skydips of the 460 GHz receiver and the on-site NRAO/CSO 225 GHz taumeter yielded an opacity ratio $\tau_{460}/\tau_{225} \sim 11.5$. The backend spectrometer was the CSO facility AOS, with a bandpass of 500 MHz, or 325 km s^{-1}. This bandwidth allows observation only of galaxies with narrow or moderately broad lines. Stable atmospheric conditions resulted in very flat baselines, and only zero-order baselines have been subtracted from the spectra.

The observations were performed by position switching symmetrically in azimuth ($\pm 180''$) at 0.1 Hz. Pointing was checked on the planets and was accurate to 3″. From maps on Mars (disk size = 16.″9) the half-power beamwidth at the ^{12}CO(4–3) frequency, $\nu = 461.040\,748$ GHz, was determined to be 1511. The temperature scale was established on Mars, assuming a 205 K disk temperature. Aperture and main-beam efficiencies were $\eta_{ap} \sim 0.36$ and $\eta_{mb} \sim 0.47$. All spectra presented are on the Rayleigh-Jeans main-beam brightness temperature scale, T_{mb}, which is corrected for atmospheric transmission and main-beam efficiency.

Spectra were measured toward the nuclei of M82, NGC 253, NGC, 6946, and IC 342 (Figures 1 and 2). For M82 and NGC 253, spectra were also obtained at offsets along the central molecular bar. For a compilation of source properties, see, e.g., Harris et al. (1991). Table 1 summarizes the sources and positions observed and the resultant line parameters. The CO(4–3) line was detected from three of the galaxies, with peak T_{mb} of 2 K (IC 342) to 5 K (M82). The line profiles are similar to those of lower J transitions obtained with similar angular resolution, any differences likely being due to 2″–3″ relative pointing

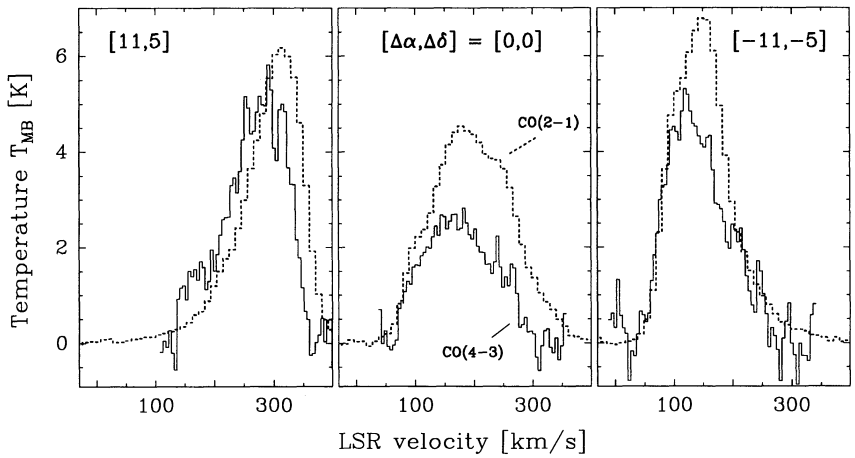

FIG. 1.—CO(4–3) spectra toward M82, box-smoothed to 4.75 km s^{-1} per channel. Offsets ($\Delta\alpha$, $\Delta\delta$) are along the nuclear major axis (P.A. 65°). For comparison, CO(2–1) spectra, smoothed to the same angular resolution of 15″, are superposed (Reuter 1991).

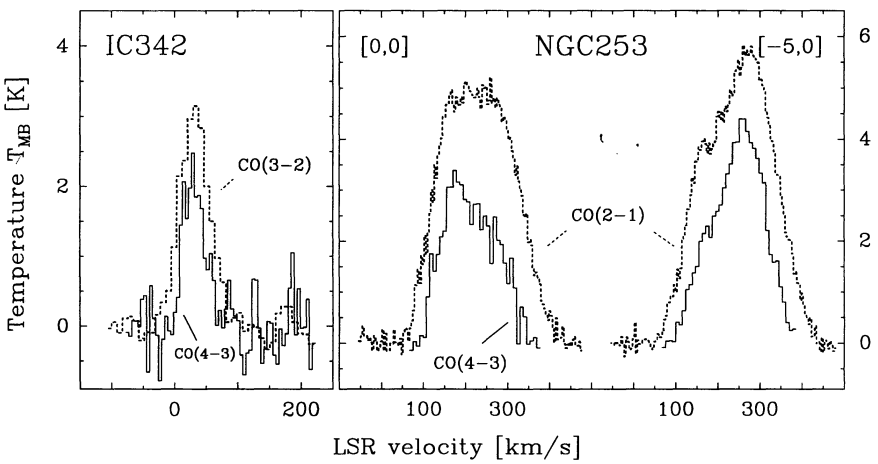

FIG. 2.—CO(4–3) spectra toward IC 342 and NGC 253, box-smoothed to 4.75 and 7.9 km s^{-1} per channel, respectively. For comparison, CO(3–2) data toward IC 342 from Steppe et al. (1990), and CO(2–1) data toward NGC 253 from Mauersberger (1991, private communication), have been convolved numerically to the same angular resolution of 15″.

offsets. For NGC 253 and its offset measurement, the zero level is difficult to determine, and the line may be underestimated. Toward NGC 6946, $T_{mb} < 0.6$ K was determined.

3. EXCITATION MODELS

The detection of the high-excitation CO(4–3) line directly indicates the presence of large amounts of warm and dense gas in these nuclei. Combined with existing data on other CO lines, the observations reveal obvious excitation differences among the galaxies: as we elaborate below, the bulk CO gas in M82 and NGC 253 is much more highly excited than in IC 342 and NGC 6946.

In Figure 3 we compile extant CO and ^{13}CO main-beam brightness temperatures for the individual sources, for all lines observed up to $J = 6$–5. A detailed excitation analysis of these data requires conversion to the true source radiation temperature, T_r, which is observationally difficult to assess. This is particularly true for spatially unresolved sources, since $T_r = T_A^*/(\eta_{mb} \cdot \eta_s \cdot \eta_{ss})$, where η_{mb} is the main beam coupling efficiency, η_s describes the large-scale coupling of a homogeneous

TABLE 1

OBSERVED POSITIONS AND RESULTS

Source	Distance (Mpc)	α_{1950}	δ_{1950}	($\Delta\alpha$, $\Delta\delta$) (arcsec)	rms (K)	T_{mb}^{peak} (K)	$\langle V_{mean} \rangle$ (km s^{-1})	$\int T_{mb}\, dV$ (K km s^{-1})
NGC 253	3.4	00^{h}45^{m}05^s.7	−25°33′38″	0, 0	0.31	3.3 ± 0.2	213	507
				−5, 0	0.13	4.2 ± 0.2	242	595
IC 342	1.8	03 41 57.2	67 56 27	0, 0	0.35	2.2 ± 0.3	32	88
M82	3.3	09 51 43.9	69 55 01	0, 0	0.25	2.5 ± 0.2	177	370
				−11, −5	0.38	4.9 ± 0.5	141	677
				11, 5	0.50	4.5 ± 0.5	263	550
NGC 6946	5.0	20 33 49.0	59 58 47	0, 0	0.15	≤0.6	...	≤100

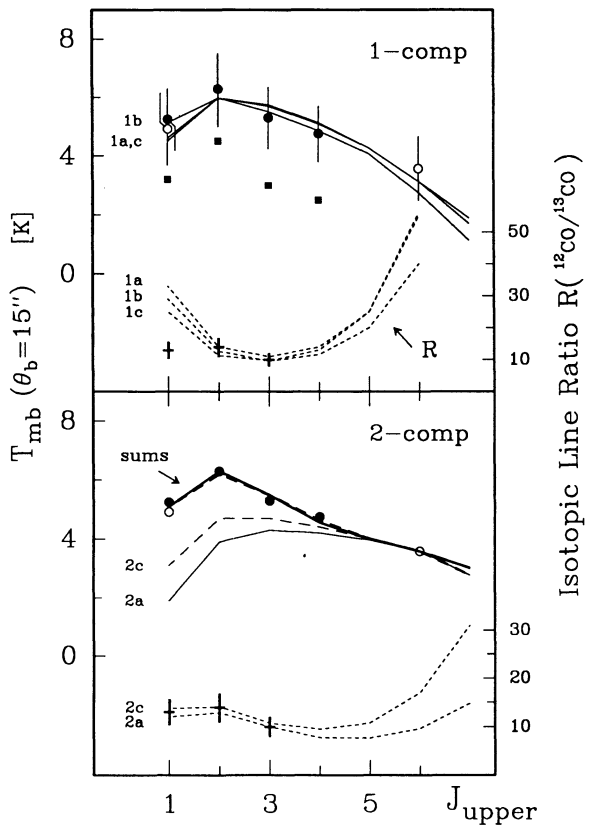

FIG. 3*a*

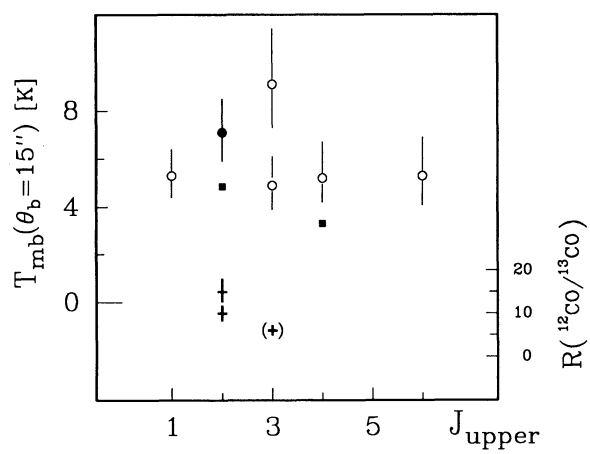

FIG. 3*b*

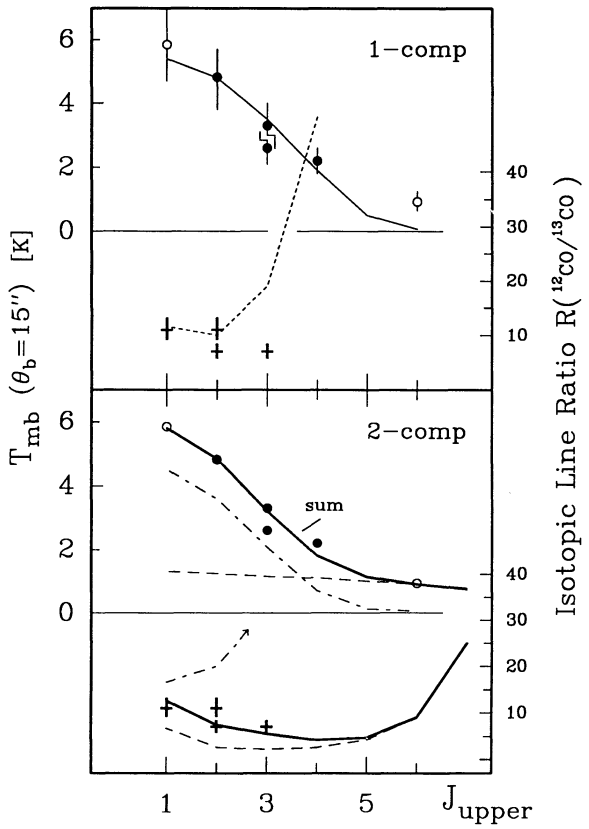

FIG. 3*c*

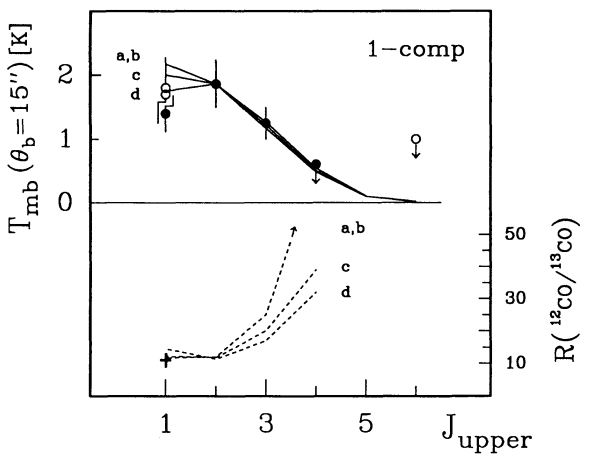

FIG. 3*d*

FIG. 3.—(*a*) Compilation of CO brightness temperatures toward M82, rescaled to a 15″ FWHP main beam, all on Rayleigh-Jeans temperature scale. Squares and circles refer to the central position and the average intensity toward the lobes, respectively. Filled symbols refer to data obtained with similar (15″ ± 2″) angular resolution; entries marked by open symbols suffer from larger source coupling corrections and should be given less weight. Isotopic line temperature ratios $R = T(^{12}CO)/T(^{13}CO)$ are presented by crosses, with their scale on the right-hand axis. *Models*: One-component LVG models (see Table 2 for model parameters) are given in the top panel (*solid lines* for CO main lines; *short-dashed lines* for isotopic lines ratios). The bottom panel displays solutions for a two-component superposition (*thick lines* representing the sum of brightness temperatures from both phases; *thin lines* outlining the emission of the hot component only; isotopic lines ratios for the combined solutions are plotted (*short-dashed*) at the bottom). Data base for CO(1–0): Nakai et al. (1987; Θ_{mb} = 16″); Carlstrom (1989, 10″); for CO(2–1): Reuter (1991; 13″.5, numerically convolved into 15″ beam. Note that this carefully calibrated data yields lower temperatures than Loiseau et al. 1988); for CO(3–2): Tilanus et al. (1991; 14″); for CO(4–3): this paper; for CO(6–5): for all sources, Harris et al. [1991; (8″; 30″)]. R_{1-0} (Loiseau et al. 1988, 1991; 13″.5; Sage & Isbell 1991; 55″); R_{2-1} (Loiseau et al. 1990; 13″.5); R_{3-2} (Tilanus et al. 1991; 14″). All temperatures rescaled for coupling the 15″ main beam to a source solid angle (at a given velocity) $\Omega_s \sim 100$ arcsec^2 (Carlstrom 1989). *Uncertainties:* formal rms errors for most data typically <10%–15%; but due to systematic offsets in the calibration scales between various telescopes and uncertain coupling efficiencies, we estimate a total uncertainty of ~20%–30% in T_{mb}. (*b*) CO excitation plot toward NGC 253. Squares toward central position, circles toward redshifted lobe ($\Delta\alpha$; −5″). Data base for CO(1–0): Canzian, Mundy, & Scoville (1988), 5″.4 × 9″.5 OVRO beam; CO(2–1): Mauersberger (1991, private communication; 13″.5); CO(3–2): Bash et al. (1990; 20″); Wall et al. (1991; 22″); the CO(4–3) entry may be slightly underestimated due to insufficient baseline coverage—all coupling efficiencies to $\Omega_s \sim 200$ arcsec^2 (Canzian et al.). Isotopic line ratios: R_{2-1} (Wall et al.; Bash et al.); R_{3-2} (Wall et al.; 24″). (*c*) CO excitation plot toward IC 342. See legend for (*a*) for details. Data base for CO(1–0) and CO(2–1): Eckart et al. (1990; 13″.5 and 21″, respectively); CO(3–2): Steppe et al. (1990; 8″.5 data numerically convolved to 15″ main beam and rescaled to main-beam temperature scale); Wall & Jaffe (1990; 15″, lower point)—all coupling efficiencies for $\Omega_s \sim 75$ arcsec^2 (Ishizuki et al. 1990a). R_{1-0}, R_{2-1} (Eckart et al.); R_{3-2} (Wall & Jaffe 1990; 24″). For *model* parameters, see Table 2. For the two-component solution (*bottom*), the emission from each component is given separately (*short-long dashed*: low-excitation phase; *long dashed*: high-density phase). (*d*) CO excitation plot toward NGC 6946. See legend for (*a*) for details. Data base for CO(1–0): Sofue, Doi, & Ishizuki (1990; 17″); CO(2–1): Götz (1990; 13″.5″); CO(3–2): Rosenthal et al. (1990; 15″), coupling efficiencies to $\Omega_s \sim 50$ arcsec^2 (Ishigura et al. 1990b). R_{1-0} (Sage & Isbell 1991; 55″). *Model* parameters are given in Table 2.

source to the main beam, and η_{ss} allows for small-scale structure (clumping) with the source. The main-beam temperature scale used in the figures is $T_{mb} = T_A^*/\eta_{mb}$. In the following, the large-scale coupling of the source to the main beam is assumed to be given by the Gaussian approximation, in which $\eta_s = \Theta_s^2/(\Theta_s^2 + \Theta_{mb}^2)$, where Θ_s and Θ_{mb} are the Gaussian source and main beam half-power widths, respectively. For our data set, η_s was inferred from interferometric or high angular resolution single-dish observations. The small-scale clumping, η_{ss}, is observationally undetermined, but, for the purposes of our modeling, is assumed to be same for all transitions for a given gas component.

Given all of these coupling parameters, uncertainties are best minimized by comparing, whenever possible, data obtained with similar angular resolutions. We therefore base our analysis preferentially on CO(1–0) data from NRO ($\Theta_{mb} = 16''$), CO(2–1) from the IRAM 30 m (13″), CO(3–2) from the JCMT (14″), and CO(4–3) from our CSO (15″) data. However, the CO(6–5) data were measured with a rather different beam pattern at the JCMT (a composite of an $\Theta_{mb} = 8''$ on top of 30″ error pattern; Harris et al. 1991). Even so, there is also apparently great difficulty in establishing the proper main beam temperature scale for a given telescope, since the scatter among the data compiled in Figure 3 suggest an 20% accuracy at best. Indeed, some points, repeated at the same telescope, differ from each other by up to a factor of 2 (Fig. 3*b*).

The CO excitation was first modeled in terms of a standard one-component spherical LVG radiative transfer model (Goldreich & Kwan 1974; de Jong, Chu, & Dalgarno 1975). Given the inhomogeneity of the interstellar medium in our Galaxy on 100 pc scales [$15'' = 220$ pc $\times$ (D/3 Mpc)], the assumption of uniform physical conditions is crude and yields only average gas properties. Even so, the data for some objects already require multicomponent emission layers (see below), which were modeled by summing two independent LVG fits, neglecting radiation coupling between them. Given the limited data quality and the lack of information on the true isotopic [^{12}C]/[^{13}C] ratio, and the source morphology and fine-scale structure, more sophisticated models are inappropriate for the time being.

The observed isotopic line temperature ratio $R = T(^{12}CO)/T(^{13}CO)$ is an important constraint to the line opacities, provided the true fractional abundance [^{12}C]/[^{13}C] is known. The observed isotopic line ratios compare well with values seen toward our Galactic center, for which an abundance ratio ~ 25 has been derived (e.g., Güsten et al. 1985a; Wannier 1988), providing evidence for an advanced state of chemical evolution of the central stellar population. For comparison, a ratio ~ 70 seems representative of the local ISM, and 50–60 for the inner Galaxy $4 \leq r \leq 6$ kpc (Henkel, Güsten, & Gardner 1985). The ratio applicable to starburst nuclei, which show evidence of peculiar stellar mass functions (Rieke et al. 1980), is difficult to judge. Sage, Mauersberger, & Henkel (1992) recently presented evidence for differences in the isotopic (oxygen) composition of the circumnuclear gas in M82 and NGC 253, as compared to the Milky Way, which, if due to enhanced massive star formation, likely implies a corresponding relative underabundance of (secondary) ^{13}C. We therefore treat the isotopic carbon ratio as a free parameter, testing our solutions for $30 \leq$ [^{12}C]/[^{13}C] ≤ 50.

Before discussing the excitation of each galaxy in turn, we summarize the basic characteristics of molecular excitation plots. As a function of rotational level, J, the intensity of optically thin emission from warm gas first increases for low J as $T_r \propto J^2$, then reaches a peak intensity at the transition for which the critical density, n_c, is comparable to the local H_2 density, and finally, at high J, falls off rapidly in this subthermally excited regime (excitation temperature T_{ex} < kinetic temperature T_k). For example, optically thin CO gas at $T_k = 50$ K and $n(H_2) = 2.5 \times 10^4$ cm^{-3} is brightest in the $J = 3$–2 line, and falls to about one-third of the peak brightness temperature at $J = 1$–0 and $J = 5$–4. However, if the emission is optically thick, the distribution with J will be broadened, and—in a spherical formulation of the escape probability—trapping will reduce the critical densities by the factor $(1 + \tau)$. Rapidly declining emission with J, as observed toward IC 342, then suggests rather cold and low-density excitation conditions [$n < n_c/(1 + \tau)$], while broad flat distributions like those of M82 and NGC 253 require optically thick, widely thermalized emission. Model solutions for all sources are superposed on the data in Figure 3, and model parameters are summarized in Table 2.

4. INDIVIDUAL GALAXIES

4.1. M82

The CO(4–3) data spatially resolve the emission along the central bar of M82, and, based on the comparable CO(2–1)/CO(4–3) line temperature ratio in the two offset positions (Fig. 1), indicate a similar excitation state in the two lobes. [Note that the spectrum toward the southwestern lobe reveals no evidence of the hot "CO(7–6) supercloud" reported by Harris et al. 1990]. Emission toward the central position is significantly weaker in the CO(4–3) line, consistent with a torus-like distribution of the circumnuclear gas (Nakai et al. 1987; Lo et al. 1987; Carlstrom 1989; Loiseau et al. 1990). There is no evidence for excess CO(4–3) emission from the CO(1–0) "central hot spot" (Carlstrom 1989) as might have been expected for central gas located close to a central heating source.

For the lobes, the relative uniformity of the emission with J (Fig. 3*a*) indicates optically thick emission from a widely thermalized population. The model parameters are thus difficult to constrain. A single-component model with $T_k \sim 50$ K (the dust temperature inferred by Smith et al. 1990) is, within the scatter, barely distinguishable from models with $T_k \sim 30$ K and ≥ 70 K (see Table 2, models 1a–1c, and Fig. 3*a*). To keep the levels thermalized, lower (higher) temperature solutions require correspondingly increased (decreased) densities. However, at temperatures less than 30 K, the deduced brightness temperatures fall below the observed ones (after allowing for beam dilution) and the predicted $J = 6$–5 brightness is too low. For temperatures greater than 70–100 K, the peak of maximum emission shifts to excessively high J, thus underestimating the low-rotational ^{13}CO transitions (but see below).

Because of the high optical depths, $\tau_{2-1} \sim 4$–5, needed to broaden the excitation plot of the main isotope (via line trapping; see § 3), isotopic abundance ratios of ~ 60 are required to fit the observed isotopic line ratios, and abundance ratios of less than 50 are difficult to reconcile with the data. Our analysis clearly excludes optically thin low-J emission that was deduced from the increase of brightness temperature between the $J = 1$–0 and 2–1 transitions (e.g., Loiseau et al. 1988, 1990), a conclusion consistent with the revised calibration for the lower J lines given by Reuter (1991; see our Fig. 3*a*). Inspection of the currently available isotopic C^{18}O data also implies opti-

TABLE 2

MODEL PARAMETERS

Source	Model Number	$n(H_2)$ [cm^{-3}]	T_k (K)	$\langle N/\Delta V\rangle$ (cm^{-2}/km s^{-1})	$\eta_s\eta_{ss}$	$^{12}C/^{13}C$	Mass Fraction
M82 (lobes)	1a	2 (4)	50	1.7 (16)	0.16	60	1.0
	1b	1 (5)	30	1.8 (16)	0.26	60	1.0
	1c	1 (4)	70	1.8 (16)	0.12	60	1.0
	2a	1 (5)	70	1.2 (16)	0.07	50	0.43
	2a	1 (3)	25	1.6 (16)	0.16	...	0.57
	2b	1 (5)	70	7.6 (15)	0.08	30	0.47
	2b	1 (3)	25	8.6 (15)	0.26	...	0.53
	2c	1 (5)	50	1.1 (16)	0.12	50	0.42
	2c	7 (2)	20	1.5 (16)	0.16	...	0.58
	2d	1 (6)	50	1.0 (16)	0.10	50	0.38
	2d	1 (3)	20	1.8 (16)	0.18	...	0.64
IC 342	1a	2 (3)	30	1.8 (16)	0.28	50	1.0
	2a	2 (4)	50	1.9 (16)	0.03	50	0.66
	2a	1 (3)	33	1.0 (16)	0.30	...	0.34
NGC 6946	1a	2 (3)	25	7.2 (15)	0.14	50	1.0
	1b	1 (3)	35	8.0 (15)	0.12	50	1.0
	1c	1.7 (3)	35	4.0 (15)	0.14	30	1.0
	1d	5 (3)	25	3.1 (15)	0.15	30	1.0

NOTES.—Parameters used in spherical LVG-models to calculate the excitation solutions in Figs. 3*a*–3*d*. Single-component solutions are numbered 1*, while two-component solutions are labeled 2*. The H_2 density $n(H_2)$, kinetic temperature T_k, beam-averaged ($\Theta_{mb} = 15''$) CO column density per linewidth $\langle N/\Delta V\rangle$, source filling factor $\eta_s\eta_{ss}$, adopted carbon isotopic abundance $^{12}C/^{13}C$, and the mass fraction for each component are listed.

cally thick main line emission (Sage et al. 1992 and Wild 1990 derive isotopic line ratios, $^{12}CO/C^{18}O \leq 60$, compared to an expected isotopic abundance ratio of $\sim$500). These conclusions compare well with those of Wild (1990), using a different radiative transfer approach. However, our derived temperatures and densities are higher than those found by Tilanus et al. (1991) based only on $J \leq 3$ data; thus emphasizing the need for a data based as complete as possible.

The crucial failure of the outlined single-component approach is its underestimate of the $^{13}CO(1–0)$ brightness (Fig. 3*a*): when the column density and density are tuned to match the 2–1 and 3–2 line ratios, the predicted ratio $R_{1-0} \sim 25–30$ is severely discrepant from the well-determined observational ratio of $\sim$13 (Fig. 3*a*; top). Also, no well-defined emission peak is predicted at $J = 2–1$, as is seen best toward the central position, but within the data noise its significance may be disputed. The model is thus obviously lacking in low-excitation material. Flattening the ^{13}CO distribution by going to optically thick isotopic lines requires excessive opacities and CO column densities, which then cannot be fitted to the observed isotopic line ratios. We conclude then, that there is no single-phase solution to the full data set.

However, the next level of approximation, a simple two-component superposition of independent LVG solutions can account for *all* of the observed constraints. In this simplified approach, the predicted line temperatures for both phases are simply co-added, and no radiation coupling is considered—a procedure that is justified only if the components are separated spatially, and along different lines of sight and are noninteracting radiatively. For spatially co-existing phases the submillimeter CO emission will still escape freely because of low optical depth. However, the emerging brightness temperature of the optically thick lower rotational CO lines might be affected by radiative transfer effects, by an amount that will depend sensitively on the local physical environment. Similarly, for spatially separated, but radiatively coupled layers the incident line radiation from one component may change the population of the other and vice versa. Without higher spatial resolution information about the detailed morphology of the source, this interaction is difficult to quantify, and fine tuning is ambiguous at present. A more detailed investigation of the limitations to the simple two-component superposition will be presented in § 4.3 for the IC 342 nucleus, for which a more extensive data base is available.

Several observations using high density tracing lines (e.g., Mauersberger & Henkel 1989) suggest that substantial amounts of gas reside at high density, of order 10^5 cm^{-3}. Our best-guess model presented in Figure 3*a* (bottom panel) adopts this density, with a temperature, $T_k \sim 50–70$ K, and includes a second cold component, $T_k \sim 20–30$ K and $n \sim 10^3$ cm^{-3}. All the data are matched perfectly. Source-averaged column densities, adjusted to reproduce the observed isotopic line ratios, are comparable for both components, $N(CO) \sim 5 \times 10^{18}$ cm^{-2} each (Table 2, models 2a and 2c, using $\Delta V \sim 130$ km s^{-1}). Solutions are possible for both sets of adopted isotopic abundances, $[^{12}C]/[^{13}C] = 30$ and 50, after readjustment of the column densities and filling factors [within the model accuracy predictions of model 2a, with a ratio of 50, and model 2b (30) are indistinguishable and therefore not displayed in Fig. 3*a*]. The filling factor of the hot phase amounts to $\eta_s\eta_{ss} \sim 0.1$, typically half the value required for the cold component.

To account for the low $J = 1–0$ isotopic line ratio, $R_{1-0} \sim 13$, the low-temperature component's emission must be heavily saturated (in model 2a, $\tau_{2-1} \sim 10$, as compared with the moderate opacity in the hot medium, $\tau_{2-1} \sim 2$). Subthermal excitation with a sharp falloff in intensity for $J > 2$ is required, as otherwise (for conditions with $T_k > 30$ K and $n >$ a few 10^3

cm^{-3}) too much population is shifted into higher levels, and the residual brightness temperature distribution cannot be fitted by feasible solutions of warm dense emission. Subthermal excitation can result from low density or temperature, and so the effects of temperature and density are difficult to disentangle. Indeed, models with (40 K, 400 cm^{-3}) or (15 K, 3×10^3 cm^{-3}) do equally well. In fact, only $T_k \cdot n^{1/2}$ is actually well constrained, with the observed line brightness implying $T_k \geq$ 15–20 K (Lo et al. 1987; Carlstrom 1989), and with the volume-averaged density of the gas yielding $n >$ a few 100 cm^{-3}. The finding that the product $T_k \cdot n^{1/2}$, instead of the pressure $T \cdot n$, is (locally) conserved between models for optically thick subthermally excited CO can be verified analytically in a two-level approximation, and thus is not an artifact of our radiative transfer handling.

In our models 2a–2c, the population of the warm component is thermalized in the lower transitions, therefore the decomposition is insensitive to our choice of density $n > 10^5$ cm^{-3} and temperature $T >$ 50–70 K. In fact, a nice model fit can be derived for 50 K and 10^6 cm^{-3}, but given independent evidence from high-gas density tracing molecules (Mauersberger & Henkel 1989) gas with these physical parameters is unlikely to be pervasive.

As can easily be seen from Figure 3*a*, the ultimate test of our two-phase decomposition will be a measurement of either the ^{13}CO(4–3) line (but this line is difficult to observe because of atmospheric absorption) or the ^{13}CO(6–5) line, the intensity of which depends sensitively on the assumed parameters. Toward the central position, no attempt for decomposition was made, because the CO(6–5) flux is missing. However, a somewhat enhanced CO(2–1) brightness (Fig. 3*a*, top) may indicate a larger fraction of cool, low-density material along this line of sight. The total gas mass of 1.5–2.0 $\times 10^8$ $M_\odot$, deduced for the central 500 pc (assuming $X_{CO} = 8 \times 10^{-4}$), is consistent with estimates from the submillimeter dust continuum (Smith et al. 1989) and from a recent isotopic CO line study (Wild 1990).

4.2. *NGC 253*

The excitation plot resembles that for M82, but may be even more extreme, with an even higher fraction of highly excited CO. Unfortunately, the inhomogeneity of the data sample prohibits detailed analysis, but the flat intensity distribution implies optically thick emission from warm dense gas. Excitation temperatures T_{ex} closely approaching the kinetic temperature up to the highest transition observed (J = 6–5 here) require densities greater than $5 \times 10^5 (1 + \tau)^{-1} (T_k/50\ \mathrm{K})^{1/2}$ cm^{-3} (for $T_{ex} \geq 0.9 T_k$). Within the noise of the data, the one-component model derived for M82 will also closely fit NGC 253, consistent with independent findings towards this nucleus (see references in Henkel et al. 1991 and discussion in Harris et al. 1991). Any decomposition must await better calibrated data.

4.3. *IC 342*

With high-resolution interferometer data available for this nearby face-on galaxy which spatially resolve different gas components (such as cloud and intercloud gas) any single-component excitation model is obsolete. Nevertheless, we present single-component fits first for the purpose of comparison with the other galaxies which lack this detailed information (note that although interferometer maps exist also for M82, the separation of gas phases is less clear-cut; Carlstrom private communication). We then proceed to a two-phase model which takes into account the full data base.

4.3.1 *Single-Component Models*

In contrast to M82, the well-defined fall-off of ^{12}CO brightness temperatures with rotational level narrowly confines the excitation in this galaxy. The transitions up to J = 4–3 are fairly well described by a single-component with $T \cdot n^{1/2} \sim 1.3 \times 10^3$ $cm^{-1.5}$ K. The solid line in Figure 3*c*, top panel, is calculated for $n = 2 \times 10^3$ cm^{-3} and T_k = 30 K, the minimum kinetic temperature implied by the interferometric data (Ishizuki et al. 1990a, b). These model parameters are in agreement with the results presented by Eckart et al. (1990) based on only the lower two transitions. However, the predicted CO(6–5) and ^{13}CO(3–2) isotopic line temperatures fall short of the measured values [T_{mb}(6–5) < 0.1 K, but 0.9 K observed, and $R_{3-2} \sim 19$, instead of ≤ 7 observed], thus calling for an additional, high-temperature emission component which is optically thick in the mid-J transitions (see also Wall & Jaffe 1990).

Recent high-resolution inerferometric data help further constrain the source morphology. Due to its proximity (1″ = 8.7 pc at a distance of 1.8 Mpc) and face-on orientation, it has become possible to spatially separate, and partially resolve, the different gas phases. Recent results show that ^{12}CO (Ishizuki et al. 1990a, b) and ^{13}CO (Ishizuki et al. 1991; Turner & Hurt 1992) do not trace the same gas. Because of lower optical depth, the latter species requires higher excitation conditions [as do NH_3 (Ho et al. 1990) and HCN (Downes et al. 1992) because of their dipole moments] and so is found concentrated in massive molecular clouds resembling the cloud complexes seen in our Galactic center (Güsten 1989). In contrast, the ^{12}CO(1–0) emission is spatially more extended and also samples the less dense intercloud medium. The isotopic line ratio R_{1-0} (and hence the optical depth) shows strong spatial variations. Ratios inferred with 2″–5″ resolution, can be as low as ~ 5 toward the most prominent clouds, but $R_{1-0} \geq 20$ in the intercloud phase (Table 3 of Downes et al. 1992). Results obtained with lower single-dish resolution thus reflect spatial, mass-weighted averages only ($R_{1-0} \sim 11 \pm 3$; Eckart et al.).

4.3.2. *Multicomponent Models*

Confined to just the one transition, the physical state of the gas is difficult to assess from the interferometer data alone. Thus any excitation analysis must still rely on the lower resolution single-dish data, which include many of the higher rotational transitions. In Figure 3*b* a composite model is presented which takes into account all of the recent observations. The dense cloud component, filling $\sim$3% of the beam, is represented by optically thick ($\tau_{2-1} \sim 20$) emission from warm (50 K) dense (2×10^4 cm^{-3}) gas. The extended component, with $\eta_s \eta_{ss} \sim 30\%$, consists of lower density, cooler gas (10^3 cm^{-3}, 33 K). Modeled isotopic ratios, $R_{1-0} \sim 6$ (clouds), $\sim$16.5 (intercloud gas), and $\sim$11.5 (beam-averaged) match the observations. Beam-averaged ratios for the transitions, $R_{2-1} \geq 7$ and $R_{3-2} \sim 6$, compare well, within the uncertainties, with the measurements of Eckart et al. ($\sim$6–11, varying across the source) and Wall & Jaffe (1990).

The ^{13}CO emission from the "cloud" component is moderately optically thick, with $\tau_{2-1} \sim 0.7$, and $R_{2-1} \sim$ 2–3. The corresponding H_2 column density is $N(H_2) \sim 3 \times 10^{23}$ cm^{-2}. The "intercloud" gas dominates the (beam-averaged) ^{12}CO emission, but contributes only about half of the ^{13}CO(1–0) emission {since $\tau[^{13}\mathrm{CO}(1\text{–}0)] < 0.1$} and less than 1/10 of the brightness for $J \geq 4$. The temperature of the cloud component compares well with the temperature of the dust, $T_D \sim 45$ K

(Rickard & Harvey 1984) and that of the dense gas traced by NH_3, $T_k \sim 70$ K (Ho et al. 1990). Within our beam, covering the giant clouds *A*, *B*, and partially *C* (Downes et al.), most of the mass ($\sim 2.7 \times 10^6\ M_\odot$) is in the cloud component, with $\sim 1.5 \times 10^6\ M_\odot$ of intercloud gas. On larger scales of $\sim 100''$, Downes et al. (1992) estimate a total of $4 \times 10^7\ M_\odot$, most of which resides in cold low-density clouds. With masses of $\sim 10^6\ M_\odot$ and sizes of 10–15 pc, each, the clouds in IC 342 are very much like the complexes observed in the center of our Galaxy (e.g., Sgr A, Sgr B2).

Uncertainties in this two-component decomposition are difficult to estimate. As before, solutions for the (subthermally excited) intercloud gas are confined by $T \cdot n^{1/2} \sim 10^3$ only. For the cloud component, lower excitation solutions ($T < 50$ K, $n < 10^4$ cm^{-3}) yield excessive ^{13}CO(2–1) brightness; on the other hand, models with $T > 70$ K and $n > 10^5$ cm^{-3}, shift too much population into higher levels, causing difficulties in explaining the high ^{13}CO(1–0) opacities observed.

The extensive data base for the IC 342 nucleus allows a more quantitative exploration of the limits of our two-component superposition of (independent) LVG solutions, taking into account now radiative coupling between the gas layers in the iterative way described by Stutzki et al. (1988). The obvious question is, to what extent the line radiation background from one component may change the population of the other, and vice versa?

The warm dense cloud component is (collisionally) thermalized at temperatures, T_{ex}, exceeding significantly any background line radiation from the intercloud phase, and therefore is not affected noticeably. In the reverse process, the evaluation is less obvious and depends critically on the detailed source morphology: because subthermal excitation (at low excitation temperatures) is required to explain the intensity fall-off with *J* for the "intercloud" medium, this is in fact the scenario where radiative pumping by a strong (line) radiation field, T_L, may become important if $\eta_\Omega \times T_L \times e^{\tau_{ic}} > T_{ex}$(ic), where η_Ω is the fraction of the sphere that illuminates the test volume, and τ_{ic} is the optical depth in the intercloud medium. For the IC 342 nucleus we derive that the level population of the intercloud layer(s) next to the surface of a dense clump ($\eta_\Omega = 0.5$, $\tau_{ic} = 0$) *will* be controlled by the background radiation, and there will be no falloff with *J*—instead, the intensity distribution is as broad as that of the background field. For $\eta_\Omega < 0.1$ (or equivalent attenuation), however, radiative coupling becomes less important than collisional excitation. Given the 10 times larger area filling factor of the intercloud gas (Table 2), and in particular, in view of its large optical depth ($\tau_{21} \sim \tau_{32} \sim 6$), we conclude that except for a thin envelope bordering the embedded cores, the bulk of the intercloud medium will *not* be affected by radiative interaction.

4.4. *NGC 6946*

Although less data are available (in particular, information about the ^{13}CO lines is sparse) the CO excitation plot resembles that of IC 342. A lower optical depth seems implied by the comparatively weak CO(1–0) brightness. Models require moderate densities, (1–2) $\times 10^3$ cm^{-3}, and temperatures $\sim$25–35 K (the upper value corresponds to the dust temperature inferred for the source; Rickard & Harvey 1984). As the CO(4–3) brightness is only an upper limit, the models listed in Table 2 may overestimate the density and/or temperature. In models 1a–c, which were constrained to match the intensities of the $J \geq 2$ lines, and the isotopic 1–0 line ratio, the 1–0 intensity is slightly high, although still within the error bars. Lower optical depths (model 1d) fitted all the main lines, but yield a somewhat low ^{13}CO(1–0) line strength. Note that the rapid increase of predicted isotopic line ratio with $J > 3$ is simply due to the fact that the optically thin ^{13}CO lines are subthermally excited, while the CO main lines are still thermalized, via radiative trapping. The gas mass within our beam is $\sim$(2–4) $\times 10^7\ M_\odot$. Any attempt to separate the amount of underlying warm material in this nucleus will have to wait for more significant limits on the submillimeter CO lines.

5. DISCUSSION AND PERSPECTIVES

The wide range of excitation conditions covered by the large number of CO transitions now observable make this molecule a powerful tool for determining the bulk properties of the molecular gas in galactic nuclei. The value of the currently accessible submillimeter CO transitions (the $J = 4$–3 presented here, and the recently published $J = 6$–5 data of Harris et al.; the $J = 5$–4 transition is not observable from ground) is twofold: in very active, M82-like nuclei, both lines complementarily trace the excitation of the warm and dense gas, with the $J = 4$–3 filling the large gap in excitation requirements toward the higher submillimeter lines. However, in the less active majority of galaxies, the bulk of the gas exists in less extreme excitation conditions, and the CO(4–3) is likely the highest detectable transition. Our analysis of IC 342 and NGC 6946, likely representatives of this class of more "normal" nuclei, has demonstrated that the subthermally excited CO(4–3) line, when combined with the lower rotational transitions, provides tight constraints on the gas density and temperature.

Our multitransition CO excitation analysis toward M82 and IC 342 (the only nuclei for which the data base is sufficiently complete to make a two-component fit feasible) shows that one component excitation models are inappropriate to explain the data. Instead, within the framework of our superposition of LVG solutions we successfully modeled the observations with a warm dense gas phase combined with a less excited, but more extended structure. Such morphology has been directly observed in nearby IC 342, where high-resolution interferometry has spatially discriminated the different gas components. Of course, no single-phase model of the interstellar medium in the Milky Way would be considered physically correct, and it is only due to the limited data base that excitation models for extragalactic nuclei have been reduced to this level of simplicity.

Within our (bimodal) approach to a likely much wider distributon of excitation conditions, the CO excitation analysis reveals the range of densities and temperatures present in these nuclei, as well as the distribution of molecular mass among the phases, information that otherwise is difficult to infer. Observations in density- and temperature-selective tracers had revealed the existence of high temperature and density gas before, but its contribution to the total amount of gas was unsettled. The M82 (and likely the NGC 253) nucleus harbors huge amounts of dense warm gas—in mass and area filling factor comparable to that stored at lower densities and temperatures (see Table 2). The excitation seems uniform across the molecular lobes. This is different from the IC 342 nucleus, where the warm dense gas is confined to a few molecular cloud complexes. The lower excitation gas is more extended, and on scales comparable to the M82 molecular ring, holds the bulk of the gas mass (e.g., Downes et al. 1992).

There is ample discussion in the recent literature (e.g., Harris

et al. 1991; Wall & Jaffe 1990) about the physics behind these high-excitation conditions. As the two nuclei that harbor the largest amounts of excited gas (M82 and NGC 253) also reveal the highest (massive) star formation efficiencies ($L_{FIR}/M \sim 200$ $L_\odot/M_\odot$), the extent of the warm gas phase is likely causally related to the presence of the young energetic stars. While current models of (soft) UV-heating processes have difficulties explaining the efficiency of the mechanisms involved in heating large amounts of dense molecular material to 50–70 K (see Stutzki et al. 1991 for a recent review), there is undisputable observational evidence (Graf et al. 1990) for the existence of significant fractions (up to a few times 10%) of warm dense molecular gas in galactic star-forming cloud complexes (e.g., M17SW and Orion A) associated with sources of intense UV flux. From their analysis of atomic fine-structure lines, Lugten et al. (1986) estimate the UV flux density in the nucleus of M82 at $\sim 10^3$ times that observed in the local interstellar medium. The pressure that is derived for the atomic gas component in the photodissociation region, $n \cdot T \sim 10^6$–10^7 K cm^{-3}, compares with the pressure calculated for the warm dense CO, 5×10^6 K cm^{-3}, both exceeding the pressure of the low-excitation gas by about two orders of magnitude.

While there is thus evidence that the distribution of gas phases in M82-type cores is controlled by their massive star formation activity, other scenarios may be viable in less active nuclei like IC 342 and NGC 6946. The morphology of IC 342 as inferred from high-resolution interferometric studies shows no general correspondence between the (UV probing) thermal radio continuum and the molecular gas distribution (except for cloud B; see discussion in Ishizuki et al., 1990a, b, and Downes et al. 1992), which makes extensive heating by OB stars very unlikely. As the characteristics of IC 342, in particular, resemble those in the center of the Milky Way, a closer inspection of its physical environment seems worthwhile. While due to its close proximity, no global excitation plot of the average conditions across the central few 100 pc of our Galaxy can be derived, observations, although biased toward selected massive cloud complexes, have revealed a similarly wide distribution of physical conditions in these clouds. From their CO excitation study, Genzel et al. (1990) find temperatures ≤ 40 K and densities $\leq 10^4$ cm^{-3} in a small sample of clouds. Symmetric top molecules reveal somewhat higher bulk temperatures (~ 50 K; Güsten et al. 1985b) with a significant fraction of the gas at higher temperatures. Similarly, analysis of density tracing molecules suggests that a few times 10% of the gas resides at $\sim 10^5$ cm^{-3}, with lower bulk densities of ~ 5000 cm^{-3} (Walmsley et al. 1986). Notably, the warm dense phase is pervasive and not related to local star formation activity, but requires instead large-scale heating mechanisms. Dissipation of turbulence (one of the outstanding characteristics of Galactic center clouds is their exceptionally large internal velocity dispersion), driven by differential galactic rotation, is a likely process (Wilson et al. 1982; Güsten et al. 1985b). From a similar analysis of the heating and cooling rate for the IC 342 molecular clouds, Downes et al. (1992) conclude that indeed heating by dissipation of kinetic energy is a more likely process than heating by stellar radiation. The efficiency of this process may depend on the local gravitation field gradients and may be enhanced by perturbed kinematics in strong barlike potentials (Harris et al 1991).

Obviously, morphological correlation studies are required to further address these different scenarios, and in fact, the sensitivity of submm facilities will soon allow follow-up observations of CO(4–3) in the vast number of other galaxies that have already been observed in their lower rotational transitions.

We are grateful to T. Phillips for granting observing time at the CSO 10.4 m telescope. Without the outstanding support from the CSO technical staff, and from MPIfR Technical Division IV in preparing the receiver, the success of this experiment would not have been possible. R. Mauersberger and H.-P. Reuter provided data prior to publication. D. Downes and A. Harris provided valuable comments on the manuscript. J. Stutzki made available his radiative transfer code for radiatively coupled layers. The CSO is supported by NSF grant AST 90-15132.

REFERENCES

Bash, F. N., Davis, J. H., Jaffe, D. T., Wall, W. F., & Sutton, E. C. 1990, in Submillimetre Astronomy, ed. G. D. Watt & A. S. Webster (Dordrecht: Kluwer), 227
Canzian, B., Mundy, L. G., & Scoville, N. Z. 1988, ApJ, 333, 157
Carlstrom, J. E. 1989, Ph.D. thesis, Univ. California Berkeley
de Jong, T., Chu, S. I., & Dalgarno, A. 1975, ApJ, 199, 69
Downes, D., Radford, S. J. E., Guilloteau, S., Guelin, M., Greve, A., & Morris, D. 1992, A&A, in press
Eckart, A., Downes, D., Genzel, R., Harris, A. I., Jaffe, D. T., & Wild, W. 1990, ApJ, 348, 434
Genzel, R., Stacey, G. J., Harris, A. I., Townes, C. H., Geis, N., Graf, U. U., Poglitsch, A., & Stutzki, J. 1990, ApJ, 356, 160
Goldreich, J., & Kwan, J. 1974, ApJ, 191, 93
Götz, M. 1990, Ph.D. thesis, Universität Bonn
Graf, U. U., Genzel, R., Harris, A. I., Hills, R. E., Russell, A. P. G., & Stutzki, J. 1990, ApJ, 358, L49
Güsten, R. 1989, in IAU Symp. 136, The Center of the Galaxy, ed. M. Morris (Dordrecht: Kluwer), 89
Güsten, R., Henkel, C., & Batrla, W. 1985a, A&A, 149, 195
Güsten, R., Walmsley, C. M., Ungerechts, H., & Churchwell, E. 1985b, A&A, 142, 381
Harris, A. I., Hills, R. E., Stutzki, J., Graf, U. U., Russell, A. P. G., & Genzel, R. 1991, ApJ, 382, L75
Harris, A. I., Wild, W., Stutzki, J., Jaffe, D. T., Jackson, J. M., Eckart, A., Lugten, J. B., & Genzel, R. 1990, preprint
Henkel, C., Baan, W. A., & Mauersberger, R. 1991, Astron. Astrophys. Rev., 3, 47
Henkel, C., Güsten, R., & Gardner, F. F. 1985, A&A, 143, 148
Ho, P. T. P., Martin, R. N., Turner, J. L., & Jackson, J. M. 1990, ApJ, 355, L19
Ishizuki, S., Kawabe, R., Ishiguro, M., Okumura, S. K., Morita, K.-I., Chikada, Y., & Kasuga, T. 1990a, Nature, 344, 244
Ishizuki, S., Kawabe, R., Ishiguro, M., Okumura, S. K., Morita, K.-I., Chikada, Y., Kasuga, T., & Doi, M. 1990b, ApJ, 355, 436
Ishizuki, S., Kawabe, R., Ishiguro, M., Okumura, S. K., Morita, K.-I., Chikada, Y., Kasuga, T., & M. C. H. Wright 1991, in IAU Symp. 146, Dynamics of Galaxies and Their Molecular Cloud Distribution, ed. F. Combes & F. Casoli (Dordrecht: Kluwer), 272
Keen, N. J., Mischerikow, K. D., Ediss, G. A., & Perchtold, E. 1986, Electronic Letters, 22, 353
Lo, K. Y., Cheung, K. W., Masson, C. R., Phillips, T. G., Scott, S. L., & Woody, D. P. 1987, ApJ, 312, 574
Loiseau, N., Nakai, N., Sofue, Y., Wielebinski, R., Reuter, H.-P., & Klein, U. 1990, A&A, 228, 331
Loiseau, N., Reuter, H.-P., Wielebinski, R., & Klein, U. 1988, A&A, 200, L1
Lugten, J. B., Watson, D. M., Crawford, M. K., & Genzel, R. 1986, ApJ, 311, L51
Mauersberger, R., & Henkel, C. 1989, A&A, 223, 79
Mauersberger, R., Henkel, C., & Sage, L. J. 1990, A&A, 236, 63
Nakai, N., Hayashi, M., Handa, T., Sofue, Y., Hasegawa, T., & Sasaki, M. 1987, PASJ, 39, 685
Reuter, H. P. 1991, Ph.D. thesis, Universität Bonn
Rickard, L. J., & Harvey, P. M. 1984, AJ, 89, 1520
Rieke, G. H., Lebofsky, M. J., Thompson, R. I., Low, F. J., & Tokunaga, A. T. 1980, ApJ, 238, 24
Rosenthal, E., Eales, S., Stephens, S., & Lo., K. Y. 1990, in Submillimetre Astronomy, ed. G. D. Watt & A. S. Webster (Dordrecht: Kluwer), 241
Sage, L. J., & Isbell, D. W. 1991, A&A, 247, 320
Sage, L. J., Mauersberger, R., & Henkel, C. 1992, A&A, in press

Sofue, Y., Doi, M., & Ishizuki, S. 1988, PASJ, 40, 511
Smith, P. A., Brand, P. W. J. L., Puxley, P. J., Mountain, C. M., & Nakai, N. 1990, MNRAS, 243, 97
Steppe, H., Mauersberger, R., Schulz, A., & Baars, J. W. M. 1990, A&A, 233, 410
Stutzki, J., Genzel, R., Graf, U. U., Güsten, R., Harris, A. I., & Sternberg, A. 1991, in IAU Symp. 147, Fragmentation of Molecular Clouds and Star Formation, ed. E. Falgarone et al. (Dordrecht: Kluwer), 235
Stutzki, J., Stacey, G. J., Genzel, R., Harris, A. I., Jaffe, D. T., & Lugten, J. B. 1988, ApJ, 332, 379
Tilanus, R. P. J., Tacconi, L. J., Zhou, S., Sanders, D. B., Sutton, E. C., Lo, K. Y., Stephens, S. A., & Wynn-Williams, C. G. 1991, ApJ, 376, 500
Turner, J. L., & Hurt, R. L. 1992, ApJ, 384, 72
Wall, W. F., & Jaffe, D. T. 1990, ApJ, 361, L45
Wall, W. F., Jaffe, D. T., Israel, F. P., & Bash, F. N. 1991, ApJ, 380, 384
Walmsley, C. M., Güsten, R., Angerhofer, P., Churchwell, E., & Mundy, L. 1986, A&A, 155, 129
Wannier, P. G. 1989, in IAU Symp. 136, The Center of the Galaxy, ed. M. Morris (Dordrecht: Kluwer), 107
Wild, W. 1990, Ph.D. thesis, L. M.-Universität, München
Wilson, T. L., Ruf, K., Walmsley, C. M., Martin, R. N., Pauls, T. A., & Batrla, W. 1982, A&A, 115, 185